Alfarama Journal of Basic & Applied Sciences

https://ajbas.journals.ekb.eg
ajbas@sci.psu.edu.eg

Faculty of Science Port Said University

http://sci.psu.edu.eg/en/

July 2025, Volume 6, Issue III

DOI: 10.21608/ajbas.2025.386713.1256

ISSN 2682-275X

Submitted: 22/05/2025
Accepted: 18/06/2025

Pages: 321 - 341

From Deep LSTM-Based Gene Expression Modeling to microRNA Disease Association; hsa-miR-133b identified as a Potentially Functionally Conserved Tumor Suppressor Across Cancers

Loai Eletr[1,*], Hazem Elzeiny[1], Ganna Mohamed[1], Aalaa Waled[1], Abdelruhman Elshazly[1], Abdelruhman Elgebaly[1], Mostafa Herajy[2], Mohamed K. Hassan[3]

[1] Computing and Bioinformatics Program, Faculty of Science, Port Said University, Port Said, Egypt

[2] Department of Mathematics and Computer Science, Faculty of Science, Port Said University, Port Said, Egypt

[3] Biotechnology Program, Biology Division, Zoology Department, Faculty of Science, Port Said University, Port Said, Egypt

***Corresponding author:** Loai.eletr65@yahoo.com

ABSTRACT

Background: Cancer remains a global health burden, and early, accurate diagnosis is vi- tal. Most deep learning models focus on binary classification, with limited work on multiclass tasks. The roles of miRNAs in cancer have also been studied. **Objective:** This study proposed a hybrid deep learning model based on Deep Long Short-Term Memory (D-LSTM) for binary and multi-class cancer classification. The important genes identified by the model were then used to predict target miRNAs. **Methods:** The D-LSTM model was trained on GEO dataset GSE203024, covering 14 cancers, colon polyps, and normal samples. Gene selection was per- formed using ANOVA-F and CFS, and SMOTE was used to handle class imbalance. Performance was evaluated using the accuracy, precision, recall, and F1-score. miRNAs were identified using miRNet, and regulatory networks were visualized using Cytoscape. **Results:** The model achieved 98.38% accuracy (binary) and 99.88–100% (multi-class). hsa-miR-133b has been linked to 14 cancers and colon polyps, targeting CTNND1, CCNB1, and SUZ12. **Conclusion:** While demon- strating strong diagnostic potential, in silico findings require further biological validation. The comprehensive evaluation of hyperparameters, activation functions, and performance metrics of the model provides a flexible framework for cancer detection. Future studies should focus on in vivo/in vitro validation of hsa-miR-133b's clinical relevance.

Keywords: Cancer; Deep learning; Gene expression; MicroRNA .

1. INTRODUCTION

In recent years, many different technologies have been developed to detect and treat patients with cancer. Cancer remains one of the most critical public health challenges, with an estimated 2.5 million new cases and 640,038 cancer-related deaths projected in the United States in 2024, and over 3.2 million new cases and 1.7 million deaths in China, highlighting the global burden of the disease [1]. Today, women and men born in the USA have an estimated lifetime of 38% and 40%, respectively, of being diagnosed with cancer [2]. Despite significant progress in advancing molecular diagnostics and targeted therapies, classifying diverse cancer types using deep learning models, particularly in the early stages of cancer development, remains a persistent challenge [3]. The detection of patients with cancer using gene expression data has proven to be an effective approach for classifying different types of cancers, such as breast cancer, based on gene expression profiles [4]. Nonetheless, there is a lack of studies employing hybrid models that effectively classify different cancer types using both binary and multiclass classification.

MicroRNAs (miRNAs) represent a class of small non-coding RNAs that play a key role in regulating gene expression and have been frequently involved in cancer development [5]. miRNAs can act as tumor suppressors by suppressing oncogenic genes or oncomiRs by targeting tumor suppressor genes involved in apoptosis and metastasis [6]. Identifying miRNAs that are consistently dysregulated across different cancer types remains a challenge for the development of pan-cancer biomarkers. Furthermore, the combination of deep learning models with miRNA-disease association frameworks has not been extensively studied.

Deep LSTM models gene expression data by capturing sequential dependencies among genes, which enables high-accuracy pan-cancer classification and perturbation-based discovery of functionally significant biomarkers [7]. Research has demonstrated the effectiveness of Deep LSTM in cancer classification when integrated with Convolutional Neural Networks (CNNs) to identify critical features and optimize parameters for accurate gene expression data analysis [8]. Recent studies have shown that LSTM models exhibit robust performance in managing irregular and incomplete time-series data from tumor marker tests, thereby enabling early cancer detection and improving the screening accu- racy in real-world clinical settings [9].

In this study, a deep long short-term memory neural network (D-LSTM) was developed to model gene expression data, including 14 cancer types, one type of colon polyp, and one healthy type. This model achieves robust performance for both binary and multiclass tumor classification. Key genes were used to build the model and explore their linked regulatory miRNAs. This comprehensive analysis reveals has-miR-133b can act as a functionally conserved cancer inhibitor in different types of malignancies.

2. MATERIALS AND METHODS

2.1 Gene Expression Data from Human Peripheral Blood

The biological dataset (GSE203024) represents a publicly available cancer diagnostic dataset derived from peripheral blood samples. It contained expression of 50675 genes across 2845 samples using the Affymetrix Human Genome U133 Plus 2.0 Array. This dataset also included 14 different cancer types, 1 type of colon polyp, and 1 healthy type. It also contains 1547 male and 1013 female volun- teers with ages ranging from 18 to 97 years. In this study, a multi- and binary-cancer classification model was developed using a deep forward-feedback neural network to differentiate sample profiles across these 16 types and normal samples from 14 cancer types, excluding colon polyps from the bi- nary classification process. Table 1 briefly summarizes the mRNA expression dataset showing cancer types by sex.

Table 1: Summary of cancer diagnoses by gender in GSE203024 dataset

Cancer Type	M	F	Unknown Gender	Total Samples	%
Healthy	943	608	249	1800	63.25
Colon polyps	145	81	1	227	7.97
Colorectal cancer	124	81	0	205	7.20
Prostate cancer	160	0	0	160	5.62
Bladder cancer	67	40	2	109	3.83
Nasopharyngeal cancer	57	21	21	99	3.48
Breast cancer	2	61	32	95	3.34
Ovarian cancer	0	64	0	64	2.25
Cervical cancer	0	36	0	36	1.27
Endometrial cancer	0	25	0	25	0.88
Stomach cancer	15	6	2	23	0.81
Liver cancer	14	2	0	16	0.56
Kidney cancer	9	5	0	14	0.49
Testicular cancer	11	0	0	11	0.39
Pancreatic cancer	3	2	0	5	0.18
Lung cancer	2	2	0	4	0.14
Total	1547	1013	285	2845	100.00

2.2. Data Preprocessing

Figure 1 shows the steps in the data preprocessing phase. The dataset was transposed to create genes as features and samples as records. The gene IDs were replaced with their actual gene symbols, excluding all gene IDs that did not include their corresponding gene symbols, which now contains only 45782 genes out of 50675. Three columns (age, sex, and disease status) were added as additional features for further analysis. More data cleaning was performed, such as identifying and removing null values present in age and gender columns, and checking for data integrity. Next, a label encoder is applied to the three columns mentioned previously. Both gender and age columns were temporar- ily dropped to perform feature selection on the gene symbols to identify relevant genes affecting the classification process. Both Correlation-based Feature Subset Selection (CFS) approximation using feature importance from Random Forest and ANOVA-F-test were utilized by selecting the top 500 genes that were highly correlated to classifying disease classes. Figure 2a shows the number of genes that overlapped between the 2 feature selection methods for multi-class classification while in Fig- ure 2b shows overlapped genes agreed by 2 feature selection methods for binary-class classification. The age and gender columns were reinserted back into the dataset, which contained only overlapping features. Owing to the imbalance of the disease type classes, the synthetic minority oversampling technique (SMOTE) was used by up-sampling all classes except the highest one to make all dis- ease types have the same number of samples for better classification. Finally, feature scaling was performed on the dataset, and the data were split into 80% for training and 20% for testing.

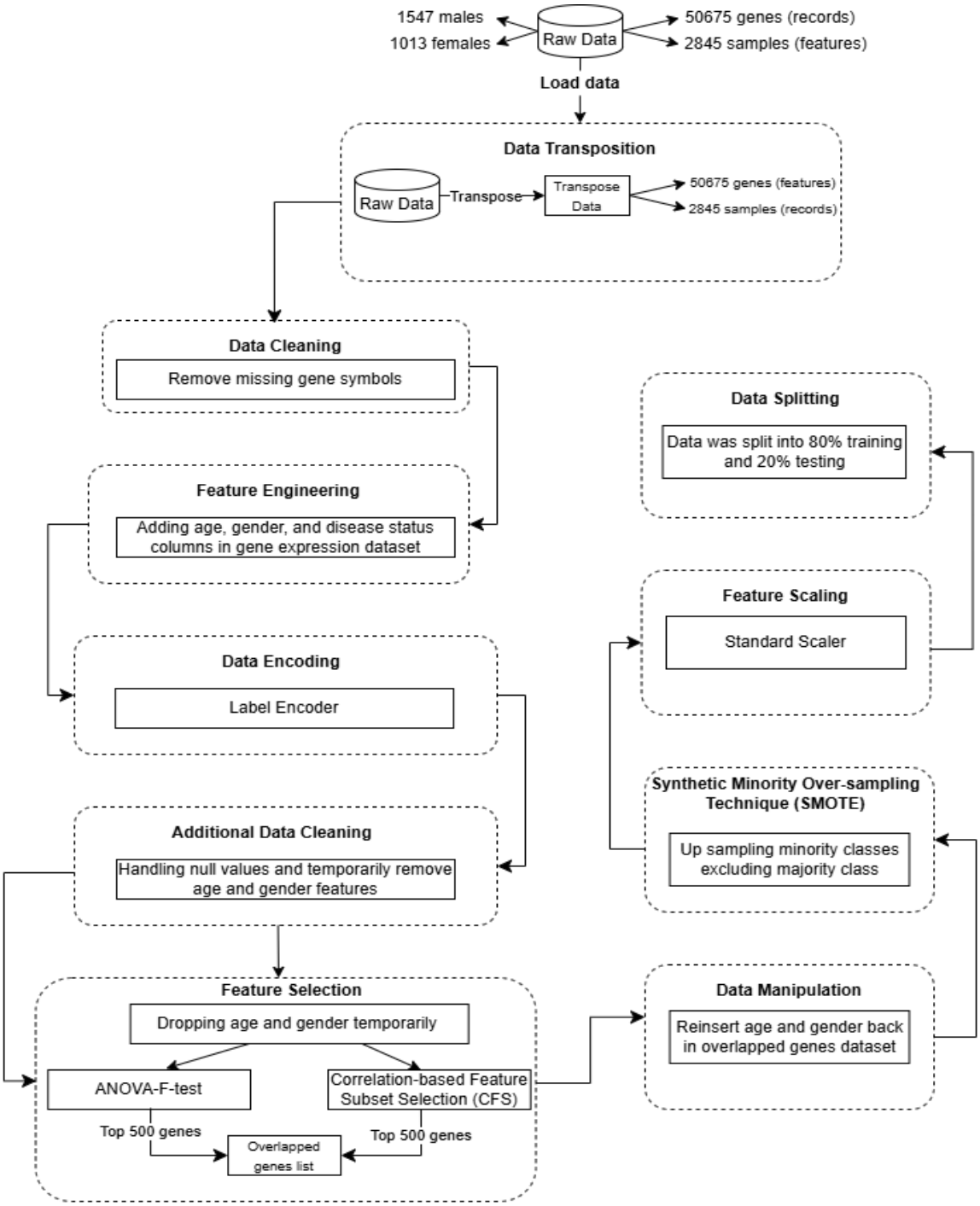

Figure 1: A comprehensive diagram that shows data preprocessing steps.

2.3. Proposed Model: Human-OncoNet

This model, Human-OncoNet, represents a deep Long Short-Term Memory neural network (D-LSTM) approach for performing both multiple and binary classification using PyTorch. It was de- signed to categorize the input data, which, in this case, were genes, into predefined classes. It har- nesses the power of both deep neural network (DNN) and LSTM. This model consists of several components: input layers, multiple LSTM layers, hidden layers with nonlinear activation functions, dropout layers for regularization, a final output layer with softmax activation for multiclass classi- fication [10], as given by (1), and sigmoid activation for binary-class classification [11], as defined in (2).

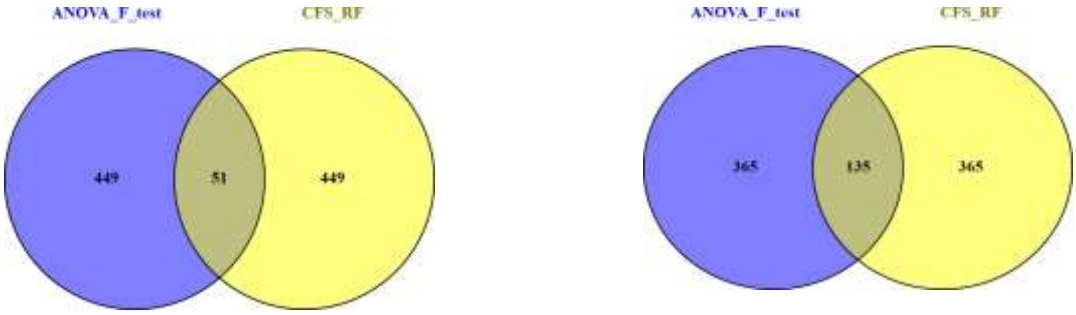

(a) The number of overlapped genes agreed by ANOVA_F_test and CFS_RF in multi-class classifi- cation.

(b) The number of overlapped genes agreed by ANOVA_F_test and CFS_RF in binary-class classi- fication.

Figure 2: Venn diagram illustration of overlapped genes for multi and binary-class classification. It depicts the most significant genes that are crucial for classifying disease status.

$$\text{Softmax}(x_i) = \frac{e^{x_i}}{\sum_{j=1}^{K} e^{x_j}} \quad \text{for} \quad i = 1,2,\ldots,K \tag{1}$$

$$\text{Sigmoid}\ (x) = \frac{1}{1 + e{-}x} \tag{2}$$

The architecture of the D-LSTM model is shown in Figures 3a and 3b used for binary and multi-class classification, respectively. The structure of the DNN model is depicted in Figures 3c and 3d which represent its configurations using both classification types. First, the input layers for the D-LSTM model passed the gene expression features to a stack of LSTM layers. These layers can capture long temporal dependencies by selectively remembering and forgetting information over a long sequence. Next, the last layer of LSTM passes its information to the first hidden layer, leading to a transition into dense (fully connected) layers. These dense layers contain hidden layers, activation functions that introduce nonlinearity to the model, and dropout layers that help prevent overfitting. Then, the output layer predicts the correct classification based on the learned patterns from the mRNA expression. The activation functions used in this study are the rectified linear unit (ReLU) [12], LeakyReLU [13], and hyperbolic tangent function (Tanh) [14], which are shown in (3), (4), and (5), respectively, and are very effective in training deep neural networks.

$$\text{ReLU}(x) = \max(0, x) \tag{3}$$

$$\text{Leaky ReLU}(x) = \begin{cases} x, & x \geq 0 \\ \alpha x, & x < 0 \end{cases} \tag{4}$$

$$\text{Tanh}(x) = \frac{e^{x} - e^{-x}}{e^{x} + e^{-x}} \tag{5}$$

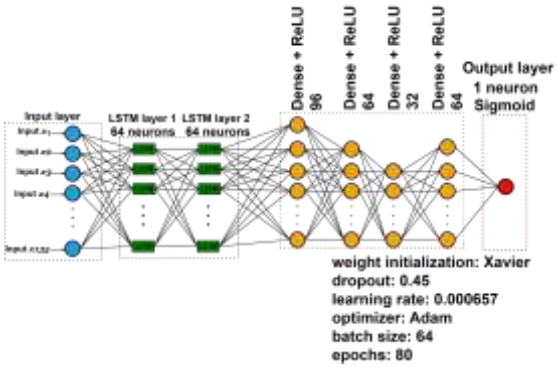

(a) Architecture of D-LSTM model for binary-class classification.

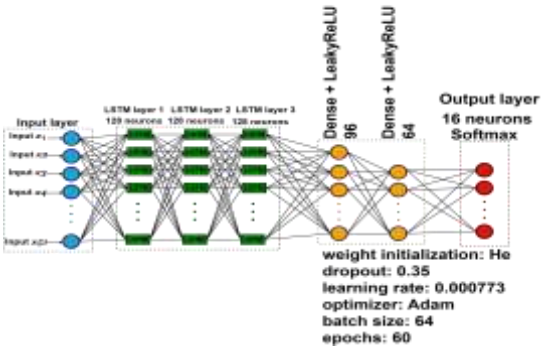

(b) Architecture of D-LSTM model for multi-class classification.

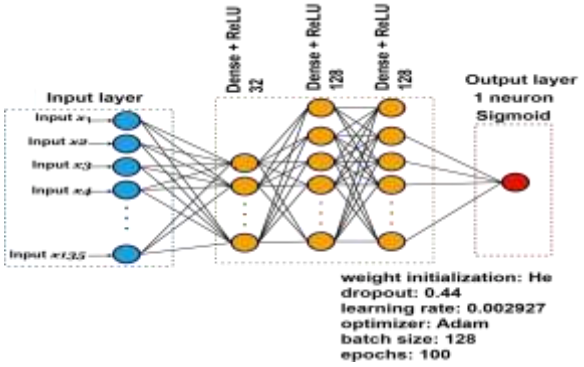

(c) Architecture of DNN model for binary-class classification.

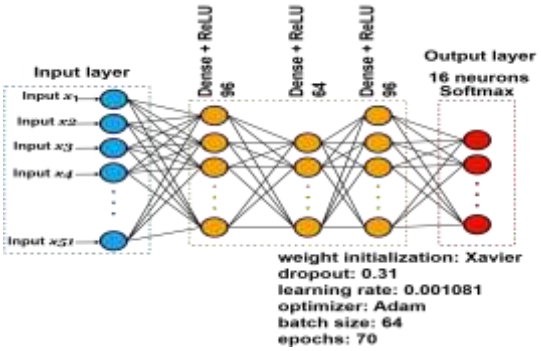

(d) Architecture of DNN model for multi-class classification.

Figure 3: The architecture of D-LSTM and DNN models.

To improve the model performance and the stability of its training, two weight initialization techniques are used: The Xavier initialization for layers with the ReLU activation function and He initialization for layers with either LeakyReLU or Tanh [15]. Several optimizers such as Adam and Stochastic Gradient Descent (SGD) [16, 17] were used to build the model.

Optuna was used for hyperparameter optimization because it uses efficient Bayesian optimization, which enables it to explore hyperparameter spaces and refine searches based on previous results. This is more advantageous than grid search, as it reduces the computational cost by stopping poorly per- forming trials early in the search, making it highly efficient for automating the hyper-tuning process. Multiple hypertuning parameters were used to perform trial and error to achieve the best parameters for both the D-LSTM and DNN models. For both models, the trained parameters were 2 to 4 hidden layers, number of neurons ranging from 32 to 128 with step size of 32, dropout rate from 0.3 to 0.5, optimizers (Adam and SGD), Activation functions (ReLU, LeakyReLU, and Tanh), batch size (64 and 128), number of epochs from 10 to 100 with step size of 10, and weight initialization (Xavier and He). In addition, an extra parameter was added to model the D-LSTM, which is the number of LSTM layers ranging from two to three, as well as the number of neurons with the same step size and number of neurons as the hidden layers. The categorical cross-entropy loss function was used for multi-classification, whereas the binary cross-entropy loss function was employed for binary classification. The best parameters for both the models are listed in Table 2.

Table 2: Best hyperparameters for D-LSTM and DNN models for binary and multi-class classification using Optuna

Task	Model Type	Number of Layers	Layer Dimensions	Dropout Rate	Learning Rate	Optimizer	Activation	Batch Size	Epochs	Weight Init	LSTM Dim	LSTM Layers	Accuracy
Binary Classification	DNN	3	[32, 128, 128]	0.46	0.002927	Adam	ReLU	128	100	He	–	–	99.68%
	D-LSTM	4	[96, 64, 32, 64]	0.45	0.000657	Adam	ReLU	64	80	Xavier	64	2	99.84%
Multi-class Classification	DNN	3	[96, 64, 96]	0.31	0.001081	Adam	ReLU	64	70	Xavier	–	–	99.38%
	D-LSTM	2	[96, 64]	0.35	0.000774	Adam	LeakyReLU	64	60	He	128	3	99.84%

2.4. Evaluation Metrics

The performance of the OncoNet model was evaluated using a confusion matrix. The evaluation metrics were calculated as follows:

$$\text{DR} = \text{TPR} = \text{Sensitivity} = \text{Recall} = \frac{\text{TP}}{\text{TP} + \text{FN}} \tag{6}$$

$$\text{TNR} = \text{Specificity} = \frac{\text{TN}}{\text{TN} + \text{FP}} \tag{7}$$

$$\text{PPV} = \text{Precision} = \frac{\text{TP}}{\text{TP} + \text{FP}} \tag{8}$$

$$\text{F1-Score} = 2 \times \frac{\text{Precision} \times \text{Recall}}{\text{Precision} + \text{Recall}} \tag{9}$$

$$\text{Accuracy} = \frac{\text{TP} + \text{TN}}{\text{TP} + \text{TN} + \text{FP} + \text{FN}} \tag{10}$$

The acronyms TP, TN, FP, and FN represent true positives, true negatives, false positives, and false negatives, respectively. Eq. (6) indicates the true positive rate (TPR) and the detection rate (DR). These metrics were used to measure how well the model recognized positive instances. Eq. (7) rep- resents the true negative rate (TNR) as it quantifies how well the model identifies negative instances. Additionally, Eq. (8) represents the positive predictive value (PPV) because it measures the pro- portion of positive predictions that are actually correct. Moreover, F1-score in Eq. (9) reveals the harmonic mean of the TPR and PPV. Eq. (10) shows the accuracy metric, which is the proportion of correct predictions to the total number of predictions made using the test data. These metrics are important for assessing machine learning models to ensure the reliability of the classification process.

2.5. Identification of Biomarkers and Construction of Regulatory Networks

After training the proposed model using important genes as features, genes that were used as fea- tures for both binary and multiclass classification were used to identify miRNAs that target these genes. The miRNet platform was suitable for this analysis because it is designed for miRNA-centered network-based analysis by providing relationships between targeted genes and associated diseases, which in this case are 14 different cancers and colon polyps [18]. After identifying miRNAs that tar- get genes associated with different cancers, a regulatory network was established using Cytoscape to visualize miRNA-gene interactions [19]. From these interactions, these findings identified important genes and miRNAs that play a key role in different cancers and potentially serve as biomarkers.

3. RESULTS AND DISCUSSION

In Section 2.4, various metrics are mentioned, such as the F1-score, accuracy, precision, and recall, to evaluate the model's performance, as described in Section 3.4. This section will focus on the metrices results to investigate how well does the 2 models able to differentiate between disease status via binary and multi-class classification tasks

3.2. Experiment configuration

For the experimental design and setup, Table 3 describes the details of the tools and setup that were used to assess various metric parameters, enabling the generation of reliable results that can be used for further analysis.

Table 3: Experiment Configuration

OS	Windows 10 Pro, 64-bit
CPU	Intel Core i7-5500U (2C/4T) @ 2.4-3.0 GHz
GPU	Intel HD Graphics 5500 (24EU)
RAM	16GB DDR3 @ 1600MHz (Dual)
Anaconda	Anaconda 2.6.5 (64-bit)
Python	Python 3.12.4 (SciPy stack)
PyTorch	PyTorch 2.3.1 (CPU)

3.3. Analysis of D-LSTM performance

As shown in Table 4, it depicts the binary classification based on the proposed models for the GSE203024 dataset used to distinguish between cancerous and non-cancerous patients based on gene expression profiles. The performance of D-LSTM is overall good, achieving high accuracy regarding differentiation between normal and cancerous samples, with accuracy of 98.38% which is slightly less than using DNN model which had an accuracy of 98.55%. Furthermore, it shows that upon differentiating gene expression samples, D-LSTM classified classes very accurately including a TPR of 98.71% and a TNR of 98.06%, which further implies capabilities of the proposed model to rec- ognize healthy patients and patients suffering from cancer. Moreover, a comprehensive analysis of the proposed model using confusion matrix was performed to allow for more visual representation of classification result, as shown in Figures 4 and 5. This study also provided a brief summary of the classification performance of the model which is depicted in Figures 6a and 6b, monitoring the model's performance over time. After each iteration, the model was evaluated on the training data and validating data while implementing an early stopping to stop the training and validating process if the validation accuracy was less than the best validation accuracy three times consecutively. This prevents the model from potential overfitting and unnecessary training. Both the D-LSTM and DNN stopped the training and validation processes at epochs 11 and 15, respectively.

Table 4: Binary classification analysis of GSE203024 dataset

Class	Model	TPR	Recall	Sensitivity	TNR	Specificity	FPR	FNR	PPV	Precision	F1	Accuracy
Cancer	DNN	100.00%	100.00%	100.00%	97.09%	97.09%	2.91%	0.00%	97.18%	97.18%	98.57%	98.55%
	D-LSTM	**98.71%**	**98.71%**	**98.71%**	**98.06%**	**98.06%**	**1.94%**	**1.29%**	**98.08%**	**98.08%**	**98.39%**	**98.38%**
Healthy	DNN	97.09%	97.09%	97.09%	100.00%	100.00%	0.00%	2.91%	100.00%	100.00%	98.52%	98.55%
	D-LSTM	**98.06%**	**98.06%**	**98.06%**	**98.71%**	**98.71%**	**1.29%**	**1.94%**	**98.70%**	**98.70%**	**98.38%**	**98.38%**

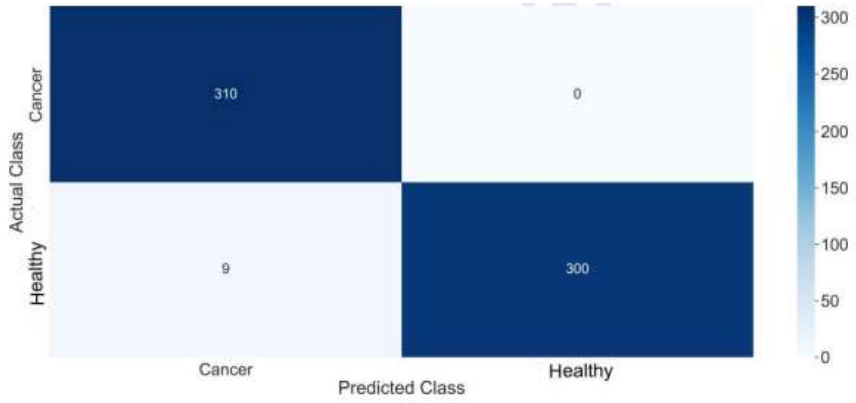

Figure 4: Confusion matrix of D-LSTM for binary classification

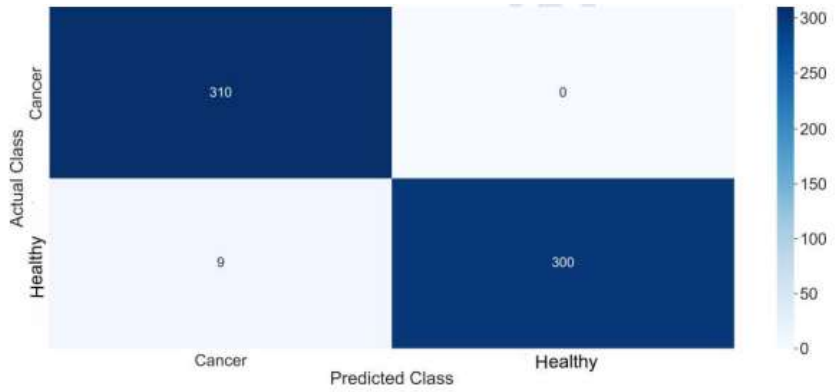

Figure 5: Confusion matrix of DNN for binary classification.

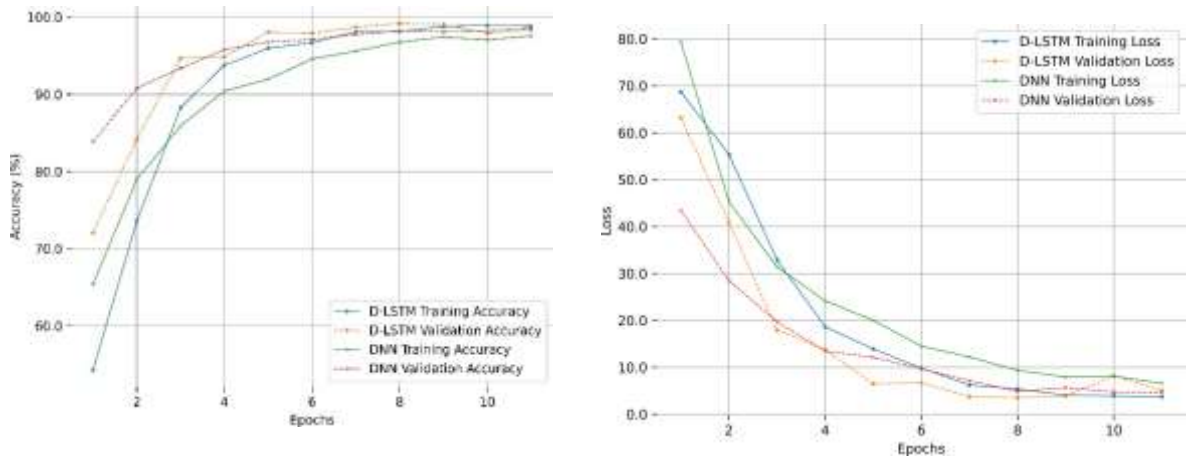

(a) Accuracy curve showing prediction outcome for training and validation data.

(b) Loss curve illustrating the distance between the true values and values predicted by the model for both train ing and validation data.

Figure 6: Training and validation accuracy and loss curves for both models on GSE203024.

Table 5: Model Performance Metrics for Various Cancer Types

Class	Model	TPR	Recall	Sensitivity	TNR	Specificity	FPR	FNR	PPV	Precision	F1	Accuracy
Bladder Cancer	DNN	99.35%	99.35%	99.35%	99.96%	99.96%	0.04%	0.65%	99.35%	99.35%	99.35%	99.92%
	D-LSTM	**99.35%**	**99.35%**	**99.35%**	**100.00%**	**100.00%**	**0.00%**	**0.65%**	**100.00%**	**100.00%**	**99.68%**	**99.96%**
Breast Cancer	DNN	100.00%	100.00%	100.00%	99.96%	99.96%	0.04%	0.00%	99.36%	99.36%	99.68%	99.96%
	D-LSTM	**100.00%**	**100.00%**	**100.00%**	**99.96%**	**99.96%**	**0.04%**	**0.00%**	**99.36%**	**99.36%**	**99.68%**	**99.96%**
Cervical Cancer	DNN	100.00%	100.00%	100.00%	100.00%	100.00%	0.00%	0.00%	100.00%	100.00%	100.00%	100.00%
	D-LSTM	**100.00%**	**100.00%**	**100.00%**	**99.98%**	**99.98%**	**0.02%**	**0.00%**	**99.68%**	**99.68%**	**99.84%**	**99.98%**
Colon Polyps	DNN	98.71%	98.71%	98.71%	100.00%	100.00%	0.00%	1.29%	100.00%	100.00%	99.35%	99.92%
	D-LSTM	**100.00%**	**100.00%**	**100.00%**	**99.96%**	**99.96%**	**0.04%**	**0.00%**	**99.36%**	**99.36%**	**99.68%**	**99.96%**
Colorectal Cancer	DNN	99.68%	99.68%	99.68%	99.96%	99.96%	0.04%	0.32%	99.35%	99.35%	99.52%	99.94%
	D-LSTM	**98.06%**	**98.06%**	**98.06%**	**100.00%**	**100.00%**	**0.00%**	**1.94%**	**100.00%**	**100.00%**	**99.02%**	**99.88%**
Endometrial Cancer	DNN	100.00%	100.00%	100.00%	100.00%	100.00%	0.00%	0.00%	100.00%	100.00%	100.00%	100.00%
	D-LSTM	**100.00%**	**100.00%**	**100.00%**	**100.00%**	**100.00%**	**0.00%**	**0.00%**	**100.00%**	**100.00%**	**100.00%**	**100.00%**
Kidney Cancer	DNN	100.00%	100.00%	100.00%	99.98%	99.98%	0.02%	0.00%	99.68%	99.68%	99.84%	99.98%
	D-LSTM	**99.68%**	**99.68%**	**99.68%**	**99.94%**	**99.94%**	**0.06%**	**0.32%**	**99.04%**	**99.04%**	**99.36%**	**99.92%**
Liver Cancer	DNN	100.00%	100.00%	100.00%	99.98%	99.98%	0.02%	0.00%	99.68%	99.68%	99.84%	99.98%
	D-LSTM	**100.00%**	**100.00%**	**100.00%**	**99.94%**	**99.94%**	**0.06%**	**0.00%**	**99.04%**	**99.04%**	**99.52%**	**99.94%**
Lung Cancer	DNN	99.68%	99.68%	99.68%	100.00%	100.00%	0.00%	0.32%	100.00%	100.00%	99.84%	99.98%
	D-LSTM	**100.00%**	**100.00%**	**100.00%**	**100.00%**	**100.00%**	**0.00%**	**0.00%**	**100.00%**	**100.00%**	**100.00%**	**100.00%**
Nasopharyngeal Cancer	DNN	100.00%	100.00%	100.00%	100.00%	100.00%	0.00%	0.00%	100.00%	100.00%	100.00%	100.00%
	D-LSTM	**100.00%**	**100.00%**	**100.00%**	**100.00%**	**100.00%**	**0.00%**	**0.00%**	**100.00%**	**100.00%**	**100.00%**	**100.00%**
Healthy	DNN	98.71%	98.71%	98.71%	100.00%	100.00%	0.00%	1.29%	100.00%	100.00%	99.35%	99.92%
	D-LSTM	**96.77%**	**96.77%**	**96.77%**	**100.00%**	**100.00%**	**0.00%**	**3.23%**	**100.00%**	**100.00%**	**98.36%**	**99.80%**
Ovarian Cancer	DNN	100.00%	100.00%	100.00%	100.00%	100.00%	0.00%	0.00%	100.00%	100.00%	100.00%	100.00%
	D-LSTM	**100.00%**	**100.00%**	**100.00%**	**99.96%**	**99.96%**	**0.04%**	**0.00%**	**99.36%**	**99.36%**	**99.68%**	**99.96%**
Pancreatic Cancer	DNN	100.00%	100.00%	100.00%	100.00%	100.00%	0.00%	0.00%	100.00%	100.00%	100.00%	100.00%
	D-LSTM	**100.00%**	**100.00%**	**100.00%**	**100.00%**	**100.00%**	**0.00%**	**0.00%**	**100.00%**	**100.00%**	**100.00%**	**100.00%**
Prostate Cancer	DNN	100.00%	100.00%	100.00%	99.94%	99.94%	0.06%	0.00%	99.04%	99.04%	99.52%	99.94%
	D-LSTM	**100.00%**	**100.00%**	**100.00%**	**99.91%**	**99.91%**	**0.09%**	**0.00%**	**98.72%**	**98.72%**	**99.36%**	**99.92%**
Stomach Cancer	DNN	100.00%	100.00%	100.00%	99.98%	99.98%	0.02%	0.00%	99.68%	99.68%	99.84%	99.98%
	D-LSTM	**100.00%**	**100.00%**	**100.00%**	**99.98%**	**99.98%**	**0.02%**	**0.00%**	**99.68%**	**99.68%**	**99.84%**	**99.98%**
Testicular Cancer	DNN	100.00%	100.00%	100.00%	100.00%	100.00%	0.00%	0.00%	100.00%	100.00%	100.00%	100.00%
	D-LSTM	**100.00%**	**100.00%**	**100.00%**	**99.98%**	**99.98%**	**0.02%**	**0.00%**	**99.68%**	**99.68%**	**99.84%**	**99.98%**

Table 5 shows the performance of the model based on its multiclass classification tasks. It is worth noting that D-LSTM showed remarkable accuracy, ranging from 99.92% to 100.00%, further demonstrating the robustness of the model in differentiating between the disease status of patients. Furthermore, the model achieved 100.00% accuracy in identifying patients with endometrial, lung, nasopharyngeal, and pancreatic cancers. All the classes had a good overall F1-score, which ranged from 99.02% to 100.00%, showing remarkable ability to distinguish between various disease types. More- over, a recall of 100.00% was achieved in terms of classifying ovarian, pancreatic, prostate, stomach, and testicular cancers, highlighting the effectiveness of the model in detecting these cancer types. To gain further insight into the accurate classification of the D-LSTM model, it is important to evaluate the results shown in the confusion matrix, as shown in Figures 7 and 8. Examining the confusion ma- trix allows a better understanding of the overall performance of the model. To verify the ability of the model to classify a validation dataset, Figures 9a and 9b show a summary of the performance of the model. Early stopping was achieved in the D-LSTM and DNN models at epochs 12 and 19. Similar to binary classification, the performance of the model was monitored by training and validating with the same early stopping strategy, similar to the approach used in binary classification.

3.3. MiRNA-gene-disease network analysis

As previously mentioned in Figure 2, this study combined the gene features used for binary and multiclass classifications, which were 51 and 135 genes, respectively. This list contained 174 genes, 12 of which were common between the two sets. These genes were submitted to the miRNet database to identify the miRNAs that target these genes. These results showed that only 79 genes were targeted by the 1425 miRNAs. Additionally, 873 miRNAs were associated with 14 different types of cancers, colon polyps, and cancer. Additional preprocessing was performed to identify the association between the 79 genes and the progression of different cancer types through miRNA regulation. However, only general cancer and 10 different types of cancer were associated with 73 out of the 79 genes through 72 miRNAs. Finally, the miRNA-gene-cancer interaction network was visualized using Cytoscope, as shown in Figure 10.

In this study, we aimed to leverage the strengths of LSTM and DNN in a single model to enhance the overall performance and accuracy of cancer detection. The proposed hybrid model improved the performance of both binary and multiclass classification tasks. Moreover, many different feature selections can be used to reduce dimensionality; therefore, ANOVA F-test and CFS were used to evaluate feature importance among the top 500 genes for both binary and multiclass classification tasks.

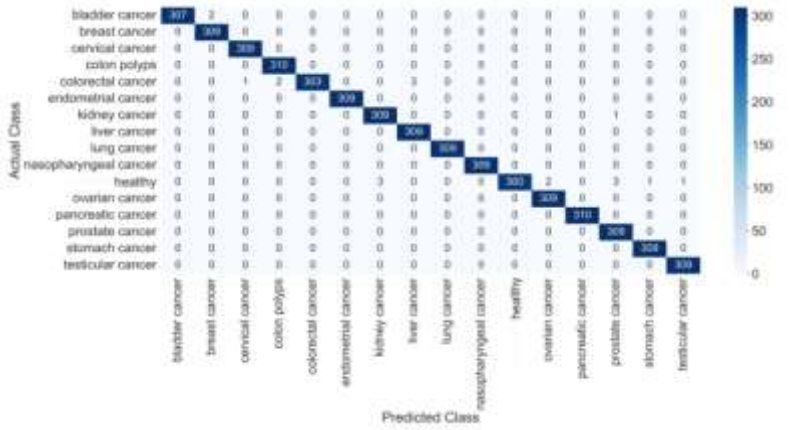

Figure 7: Confusion matrix of D-LSTM for multi-class classification.

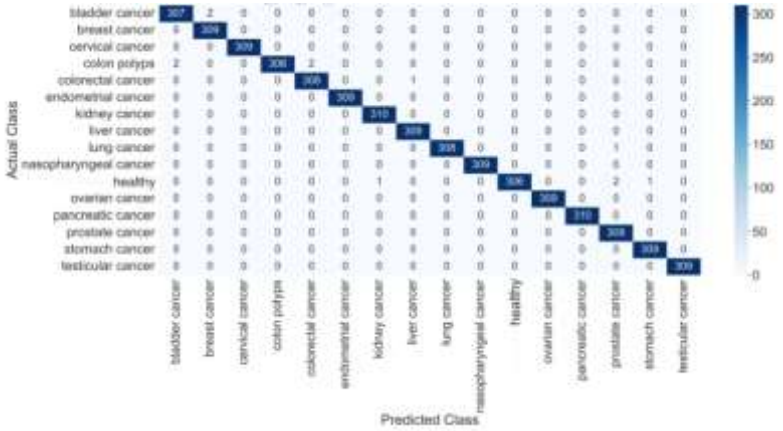

Figure 8: Confusion matrix of DNN for multi-class classification.

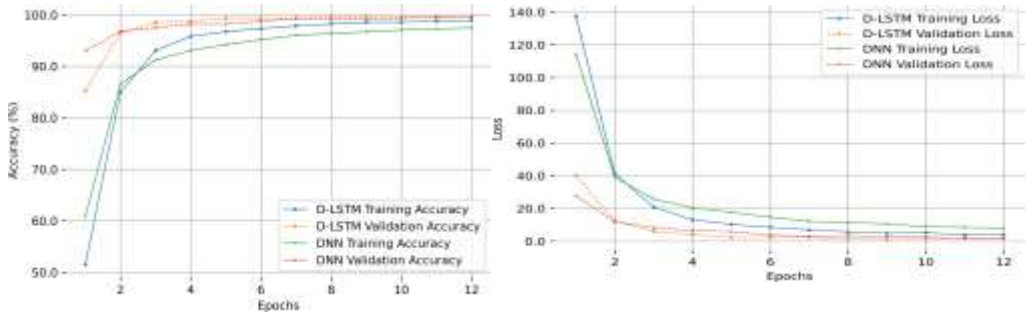

(a) Accuracy curve showing prediction outcome for training and validation data.

(b) Loss curve illustrating the distance between the true values and values predicted by the model for both training and validation data.

Figure 9: Training and validation accuracy and loss curves for both models on GSE203024 for multi- class classification.

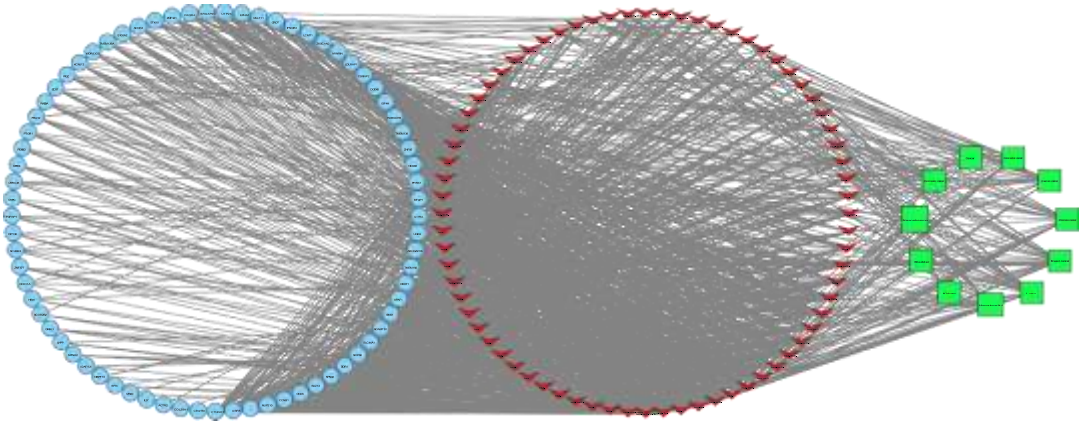

Figure 10: MiRNA-gene-cancer interaction network. The light blue circles represent genes. The red triangles indicate miRNAs. The green rectangles show different cancer types and general cancer associated with miRNAs.

The overlapping features between the two methods were determined to eliminate redundant genes that did not correlate with the distinction between different cancer types. Furthermore, when addressing class imbalance, The SMOTE method was used for up-sampling minority samples to obtain the same number as the majority sample, which in this case was healthy. Additionally, this was performed to increase the overall performance of the training and validating sets, ensuring equal importance of fea- tures to mitigate the impact of class imbalance. In addition, many different metrics such as accuracy, precision, recall, and F1-score were used to determine the performance of the model for each class. Hyperparameter tuning is a critical process in training a neural network that aids in determining the optimal set of parameters that maximizes accuracy. In this case, the Optuna technique was used to automate the hyperparameter-tuning process for the proposed model. This study experimented with different hyperparameters, such as the number of hidden layers and neurons, dropout rates, learning rates, optimizer, activation functions, batch size, epochs, weight initializations, and the number of LSTM layers, along with their corresponding number of neurons. These parameters were used to determine the optimal settings that yielded the best accuracy for the proposed model.

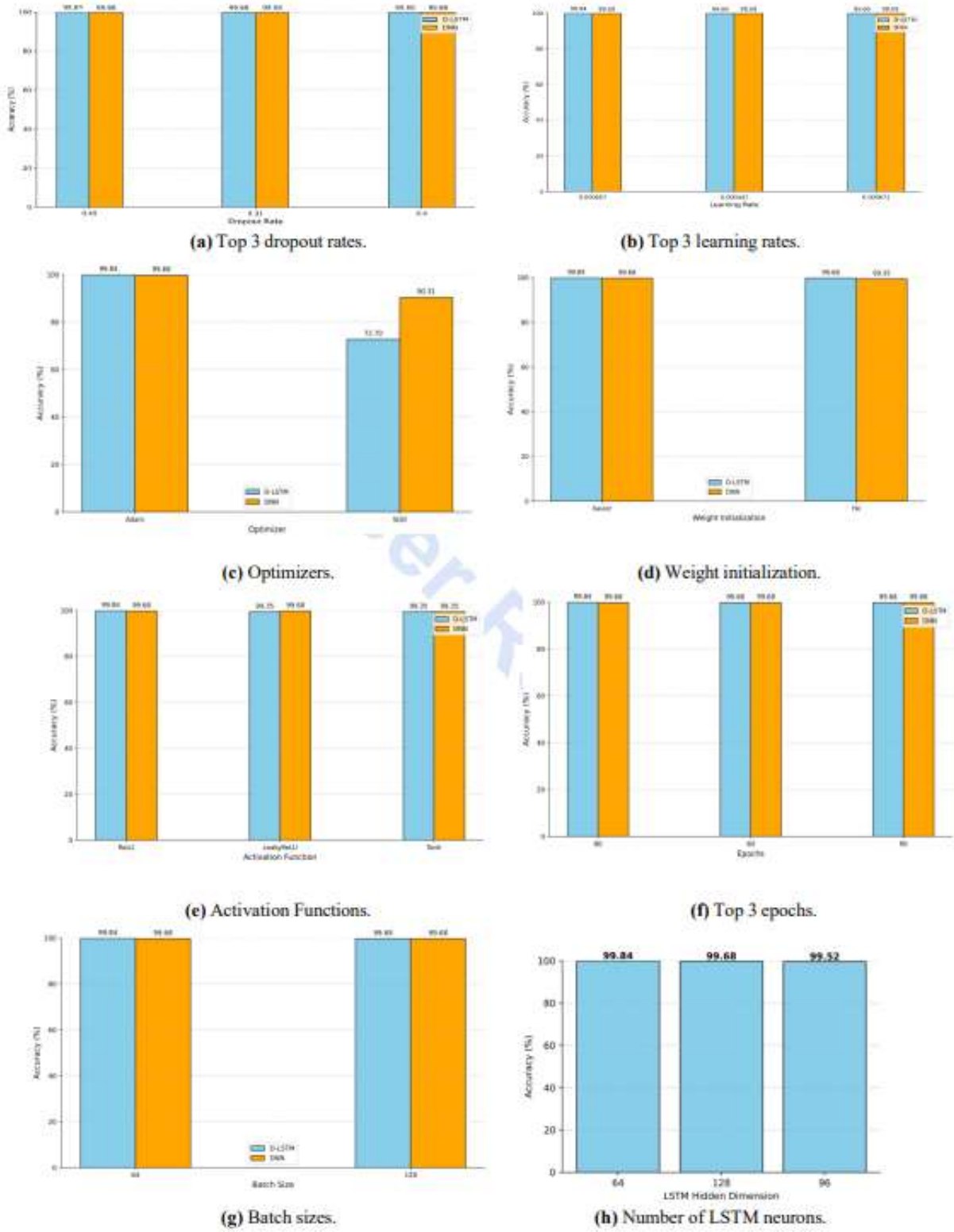

(a) Top 3 dropout rates.

(b) Top 3 learning rates.

(c) Optimizers.

(d) Weight initialization.

(e) Activation Functions.

(f) Top 3 epochs.

(g) Batch sizes.

(h) Number of LSTM neurons.

Figure 11: Comparison of model's performance with different hyperparameters using Optuna for binary classification.

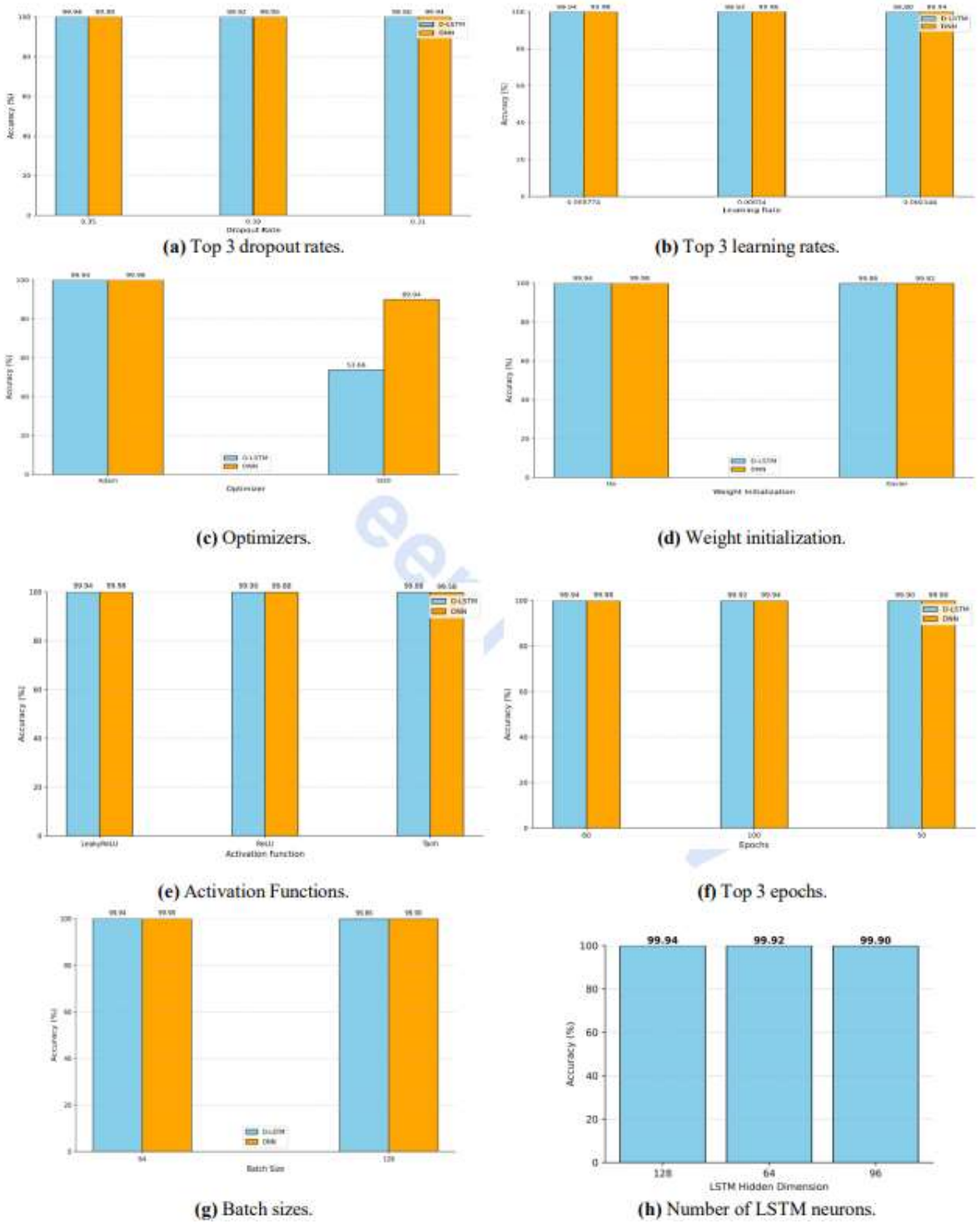

Figure 12: Comparison of model's performance with different hyperparameters using Optuna for multi-class classification.

To illustrate the performance of the different parameters for binary classification, as mentioned previously in Table 2, Figure 11a illustrates the accuracy of the model in response to the top three dropout rates of 0.45, achieving the highest accuracy. Figure 11b shows the model's accuracy in respond to top 3 learning rates with 0.000657 obtaining the best accuracy. Figure 11c shows the accuracy of the proposed

model in response to different optimizers, indicating that Adam achieved the best accuracy. Figure 11d illustrates the accuracy of the model in response to different weight initializations, with Xavier indicating optimal accuracy. In addition, Figure 11e shows the performance of the model corresponding to different activation functions, with ReLU as the parameter that achieved the highest accuracy. Furthermore, Figure 11f indicates the accuracy of the model in response to the top three epochs, with 60 epochs achieving the highest accuracy. Figure 11g shows the performance of the model using different batch sizes of 64 to obtain the best accuracy. Furthermore, Figure 11h shows the performance of the model using 64 LSTM neurons, which achieved the best accuracy. For mul- ticlass classification, these hyperparameters are illustrated in Figures 12a through 12h with the same approach as binary classification, where the different parameters are explicitly explained in detail.

The proposed Human-OncoNet is a deep LSTM-based model for binary classification of cancer in human samples based on peripheral blood gene expression profiles. The model demonstrates the ability to classify the presence of cancer with an accuracy of 98.38%, precision of 98.08%, recall of 98.71%, and F1-score of 98.39%. Together, these metrics show that the model effectively de- tects and differentiates cancerous and non-cancerous samples with balanced true-positive and true- negative samples. The model consistently distinguished between classes with low false-positive and false-negative rates. Furthermore, it is valuable to consider other methods of evaluation, namely sen- sitivity, specificity, precision, and F1-score, which are more comprehensive methods of evaluation than accuracy alone. In the multi-class classification context, Human-OncoNet was shown to be ex- ceptionally effective within a cohort comprising 14 different cancer types, in addition to a healthy class of samples, based on gene expression data derived from peripheral blood. The LSTM-based model provided an overall accuracy of 99.94% and the F1-scores for the cancer types individually ranged from 98.36% to 100%. Generally, the precision and recall metrics for most cancer types were

> 99%, indicating that the model was highly balanced and characterized by minimal false negative and false positive classifications. However, the model achieved a 100% F1-score and perfect recall for detecting the relevant cancer types, such as endometrial, lung, nasopharyngeal, and pancreatic cancer, which demonstrated strong distinguishing ability. These results suggest a near-perfect performance in the surgical classification context and illustrate the potential of Human-OncoNet as a non-invasive diagnostic tool for the early and accurate detection of multiple cancers based on transcriptomic data. To evaluate the effectiveness of this study, Table 6 shows a comparative analysis with different mod- els previously proposed in the literature. Compared to previous approaches, such as ANN, GRU, and Res-Net-based models, the proposed model provided consistently better recall, precision, F1 scores, and accuracy, particularly distinguishing cancerous from non-cancerous samples and differentiating between different types of cancers and colon polyps.

In this study, these findings showed that hsa-miR-107 and hsa-miR-133b were involved the most in many different types of cancer, including breast cancer, colorectal cancer, lung cancer, ovarian can- cer, pancreatic cancer, prostate cancer, hepatocellular carcinoma, and bladder cancer. Additionally, CTNND1, CCNB1, ZMYM2, and SUZ12 were targeted by the highest number of miRNAs involved in different types of cancer, underscoring their central role in cancer. hsa-miR-107 act as a tumor- suppressive microRNA in breast cancer [28], lung cancer [29], pancreatic cancer [30], and hepato- cellular carcinoma [31] while it acts as oncomiR in colorectal cancer [32], ovarian cancer [33], and prostate cancer [34]. From these findings, hsa-miR-107 have a multifaceted role in breast cancer by targeting both oncogenes (CTNND1, CCNB1, SUZ12) and tumor suppressor genes (ZMYM2) [35– 38]. However, in ovarian cancer, some genes, such as CTNND1 [39], act as tumor suppressor genes. It involves regulating cell-to-cell adhesion, by stabilizing cadherin/catenin complex, indicating the role of hsa-miR-107 in promoting tumorigenesis by repressing the expression of CTNND1. Moreover, the role of hsa-miR-133b remains consistent across different types of cancers. it hinders cancer pro- gression in breast cancer [40], hepatocellular carcinoma [41], ovarian cancer [42], lung cancer [43], pancreatic cancer [44], colorectal cancer [45], prostate cancer [46], and bladder cancer [47]. It targets a range of genes including CTNND1, CCNB1, ZMYM2, and SUZ12. By investigating the role of genes and their targeted miRNAs, This study uncovered that the miRNA hsa-miR-133b consistently exhibits tumor suppressor activity across these cancers and plays an important role in cell proliferation and apoptosis [48], suggesting its potential as a functionally conserved biomarker in cancer research. However, further investigations regarding its expression in wider variety of cancers are required

Despite the promising outcomes of this study, several limitations should be acknowledged. For exam- ple, the number of samples is relatively small (2845 samples) used for training and validating the deep

learning model, leading to limiting the generalization of the model across different cancer types. Another issue is the several class imbalances in the dataset, which were mitigated by applying SMOTE to handle class imbalance. Although SMOTE is an effective method for balancing class representation, it is important to note that the samples generated by it are derived from existing minority class data and may not fully reflect the true biological variation. Consequently, there is a potential risk that the model may learn patterns that are artificial and that do not exist in real-world scenarios. Another lim- iting factor is that this study used only a single gene expression dataset obtained from GEO, making it difficult to generalize the findings across different populations. Lastly, while these promising insights identified hsa-miR-133b as functionally conserved biomarker in cancer, all of the analysis was done in silico, neither in vivo or in vitro, requiring biological validation to provide clinical relevance in diagnosis or therapy. Future research should focus on performing functional experiments to confirm the role of has-miR-133b and explore its mechanism of action in diverse cancer types.

Table 6: Performance comparison of deep learning models for cancer detection

Ref	Model	Dataset	PPV	TPR	F1	Accuracy
[20]	GRU (RNN)	RNA-seq (binary)	96.8%	97.4%	97.1%	97.2%
[21]	FFN + PCA	TCGA (Kidney cancer)	97.9%	–	98.0%	98.2%
[22]	DeepCues (CNN)	WES data (7 cancer types)	–	–	–	77.6%
[23]	ANN (Pan-cancer)	Gene expression (multi-class)	96.13%	95.73%	95.60%	95.74%
[24]	ResNet-18	Dermoscopic skin cancer images	–	–	–	89.0%
[25]	ANN	Gene expression (breast cancer)	94.0%	96.0%	95.0%	95.0%
[26]	MGAN-FB	8 gene microarray datasets	97.34%	96.23%	96.72%	97.18%
[27]	APTIMA mRNA	HPV Cervical screening (meta-analysis)	–	98%	–	–
Proposed	**D-LSTM**	**Peripheral blood gene expression (GSE203024)**	**98.08%**	**98.71%**	**98.39%**	**98.38%**
	(Multiclass)	**14 cancer types + healthy + colon polyps**	**98.72–100%**	**96.77–100%**	**99.02–100%**	**99.88–100%**

3. CONCLUSION

In conclusion, this paper presents a comprehensive analysis using both binary and multiclass classification methods to ensure the success of the experiment and provides all necessary details, includ- ing accuracy, system specifications, number of hyperparameters, activation function performance, batch size performance, confusion matrix, trial performance, hidden layer performance, epoch performance, classification loss, weight initialization, dropout rate, optimizer efficiency, and multi-model

comparison. SMOTE and hyperparameter tuning techniques were applied to enhance the flexibility of the model and to facilitate a more accurate evaluation. Every component of the model was exam- ined thoroughly to assess its performance. By employing deep learning techniques, the model can detect the presence of cancer in patients and identify the specific type of cancer, thereby supporting timely and accurate diagnosis. This approach has the potential to contribute meaningfully to medical diagnostics and improve overall diagnostic methodologies.

4. ABBREVIATIONS

miRNAs	microRNAs
D-LSTM	Deep Long Short-Term Memory
USA	United States of America
CFS	Correlation-based Feature Subset Selection
SMOTE	Synthetic Minority Over-sampling Technique
DNN	Deep Neural Network
ReLU	Rectified Linear Unit
Tanh	Hyperbolic Tangent Activation Function
SGD	Stochastic Gradient Descent
TPR	True Positive Rate
DR	Detection Rate
TNR	True Negative Rate
PPV	Positive Predictive Value
ROC	Receiver Operating Characteristic
GRU	Gated Recurrent Unit
RNN	Recurrent Neural Network
FFN	Feedforward Network
PCA	Principal Component Analysis
TCGA	The Cancer Genome Atlas
ANN	Artificial Neural Network
MGAN-FB	Multi-Granularity Attention Network with Feature Boosting
APTIMA	Aptima HPV Assay (commercial nucleic acid amplification test)
HPV	Human Papillomavirus

5. REFERENCES

[1] Y. Wu, S. He, M. Cao, Y. Teng, Q. Li, N. Tan, J. Wang, T. Zuo, T. Li, Y. Zheng, C. Xia, and W. Chen, “Comparative analysis of cancer statistics in china and the united states in 2024,” Chin. Med. J. (Engl.), vol. 137, no. 24, pp. 3093–3100, Dec. 2024.

[2] R. L. Siegel, A. N. Giaquinto, and A. Jemal, “Cancer statistics, 2024,” CA Cancer J. Clin., vol. 74, no. 1, pp. 12–49, Jan. 2024.

[3] F. Alharbi and A. Vakanski, “Machine learning methods for cancer classification using gene expression data: A review,” Bioengineering (Basel), vol. 10, no. 2, p. 173, Jan. 2023

[4] R. Wesolowski and B. Ramaswamy, “Gene expression profiling: Changing face of breast cancer classification and management,” Gene Expr., vol. 15, no. 3, pp. 105–115, Oct. 2011.

[5] S. Lin and R. I. Gregory, “MicroRNA biogenesis pathways in cancer,” Nat. Rev. Cancer, vol. 15, no. 6, pp. 321–333, Jun. 2015.

[6] Y. Peng and C. M. Croce, “The role of MicroRNAs in human cancer,” Signal Transduct. Target.Ther., vol. 1, no. 1, Jan. 2016.

[7] X. Zhao, Z. Chen, H. Wang, and H. Sun, “Occlusion enhanced pan-cancer classification via deep learning,” BMC Bioinformatics, vol. 25, no. 1, p. 260, Aug. 2024.

[8] S. Ganesh and M. Nachimuthu, “Improving cancer classification using deep reinforcement learning with convolutional lstm networks,” Revue d’Intelligence Artificielle, vol. 37, pp. 1367–1376, 10 2023.

[9] X. Wu, H.-Y. Wang, P. Shi, R. Sun, X. Wang, Z. Luo, F. Zeng, M. S. Lebowitz, W.-Y. Lin, J.-J. Lu, R. Scherer, O. Price, Z. Wang, J. Zhou, and Y. Wang, "Long short-term memory model - a deep learning approach for medical data with irregularity in cancer predication with tumor markers," Comput. Biol. Med., vol. 144, no. 105362, p. 105362, May 2022.

[10] C. M. Bishop, Neural Networks for Pattern Recognition. Oxford University Press, 11 1995.

[11] F. Rosenblatt, "The perceptron: a probabilistic model for information storage and organization in the brain," Psychol. Rev., vol. 65, no. 6, pp. 386–408, Nov. 1958.

[12] V. Nair and G. E. Hinton, "Rectified linear units improve restricted boltzmann machines," in Proceedings of the 27th International Conference on International Conference on Machine Learning, ser. ICML'10. Madison, WI, USA: Omnipress, 2010, p. 807–814

[13] J. Ackermann, A. Jentzen, T. Kruse, B. Kuckuck, and J. L. Padgett, "Deep neural networks with relu, leaky relu, and softplus activation provably overcome the curse of dimensionality for kolmogorov partial differential equations with lipschitz nonlinearities in the l p-sense," 2023.

[14] T. De Ryck, S. Lanthaler, and S. Mishra, "On the approximation of functions by tanh neural networks," Neural Networks, vol. 143, p. 732–750, Nov. 2021.

[15] S. K. Kumar, "On weight initialization in deep neural networks," CoRR, vol. abs/1704.08863, 2017.

[16] D. P. Kingma and J. Ba, "Adam: A method for stochastic optimization," 2017.

[17] L. Bottou, "Large-scale machine learning with stochastic gradient descent," in Proceedings of COMPSTAT'2010, Y. Lechevallier and G. Saporta, Eds. Heidelberg: Physica-Verlag HD, 2010, pp. 177–186.

[18] L. Chang, G. Zhou, O. Soufan, and J. Xia, "mirnet 2.0: network-based visual analytics for mirna functional analysis and systems biology," Nucleic Acids Research, vol. 48, no. W1, pp.W244–W251, 06 2020.

[19] P. Shannon, A. Markiel, O. Ozier, N. S. Baliga, J. T. Wang, D. Ramage, N. Amin, B. Schwikowski, and T. Ideker, "Cytoscape: a software environment for integrated models of biomolecular interaction networks," Genome Res, vol. 13, no. 11, pp. 2498–2504, Nov. 2003. S. Babichev, I. Liakh, and I. Kalinina, "Applying a recurrent neural network-based deep learning model for gene expression data classification," Applied Sciences, vol. 13, no. 21, 2023.

[20] O. A. Razzaq, "Investigation of machine learning on gene expression data for cancer detection," Math. Model. Eng. Probl., vol. 11, no. 9, pp. 2368–2376, Sep. 2024

[21] Z. Zeng, C. Mao, A. Vo, X. Li, J. O. Nugent, S. A. Khan, S. E. Clare, and Y. Luo, "Deep learning for cancer type classification and driver gene identification," BMC Bioinformatics, vol. 22, no. Suppl 4, p. 491, Oct. 2021

[22] C. Cava, C. Salvatore, and I. Castiglioni, "Pan-cancer classification of gene expression data based on artificial neural network model," Appl. Sci. (Basel), vol. 13, no. 13, p. 7355, Jun. 2023.

[23] H. Hussein, A. Magdy, R. Abdel-Kader, and K. Ali, "Binary classification of skin cancer using pretrained deep neural networks," Suez Canal Engineering, Energy and Environmental Science, vol. 1, no. 2, pp. 10–14, Jul. 2023.

[24] C. A. Kumar and S. Ramakrishnan, "Binary classification of cancer microarray gene expression data using extreme learning machines," in 2014 IEEE International Conference on Computational Intelligence and Computing Research, 2014, pp. 1–4.

[25] M. Arbyn, M. Simon, S. de Sanjosé, M. A. Clarke, M. Poljak, R. Rezhake, J. Berkhof, V. Nyaga, M. Gultekin, K. Canfell, and N. Wentzensen, "Accuracy and effectiveness of HPV mRNA testing in cervical cancer screening: a systematic review and meta-analysis," The Lancet Oncology, vol. 23, no. 7, pp. 950–960, Jul. 2022.

[26] Y. Zeng, Y. Zhang, Z. Xiao, and H. Sui, "A multi-classification deep neural network for cancer type identification from high-dimension, small-sample and imbalanced gene microarray data," Scientific Reports, vol. 15, no. 1, p. 5239, Feb. 2025.

[27] J. Zhou, X. Sun, X. Zhang, H. Yang, Z. Jiang, Q. Luo, Y. Liu, and G. Wang, "mir-107 is involved in the regulation of NEDD9-mediated invasion and metastasis in breast cancer," BMC Cancer, vol. 22, no. 1, p. 533, May 2022.

[28] Y. Fan, H. Li, Z. Yu, W. Dong, X. Cui, J. Ma, and S. Li, "Long non-coding RNA FGD5-AS1 promotes non-small cell lung cancer cell proliferation through sponging hsa-mir- 107 to up-regulate FGFRL1," Biosci. Rep., vol. 40, no. 1, Jan. 2020.

[29] K.-H. Lee, C. Lotterman, C. Karikari, N. Omura, G. Feldmann, N. Habbe, M. G. Goggins, J. T. Mendell, and A. Maitra, "Epigenetic silencing of MicroRNA mir-107 regulates cyclin-dependent kinase 6 expression in pancreatic cancer," Pancreatology, vol. 9, no. 3, pp. 293–301, Apr. 2009.

[30] H.-A. Chen, C.-C. Li, Y.-J. Lin, T.-F. Wang, M.-C. Chen, Y.-H. Su, Y.-L. Yeh, V. V. Padma, P.-H. Liao, and C.-Y. Huang, "Hsa-miR-107 regulates chemosensitivity and inhibits tumor growth in hepatocellular carcinoma cells," Aging (Albany NY), vol. 13, no. 8, pp. 12 046–12 057, Apr. 2021.

[31] J. Zhang, J. Sun, J. Liu, D. Gu, and X. Shi, "Correlation between microRNA-107 expression level and prognosis in patients with colorectal cancer," Int. J. Clin. Exp. Pathol., vol. 13, no. 9, pp. 2342–2347, Sep. 2020.

[32] M. Wilczynski, M. Kielbik, D. Senderowska, T. Krawczyk, B. Szymanska, M. Klink, J. Bien´kiewicz, H. Romanowicz, F. Frühauf, and A. Malinowski, "MiRNA-103/107 in primary high-grade serous ovarian cancer and its clinical significance," Cancers (Basel), vol. 12, no. 9, p. 2680, Sep. 2020.

[33] J. Puente-Rivera, D. A. De la Rosa Pérez, S. I. N. Olvera, E. E. Figueroa-Angulo, J. G. C. Saucedo, O. Hernández-León, and M. E. Alvarez-Sánchez, "The circulating mir-107 as a potential biomarker up-regulated in castration-resistant prostate cancer," Noncoding RNA, vol. 10, no. 5, p. 47, Aug. 2024.

[34] X.-H. Gao, Y.-L. Zhang, Z.-Y. Zhang, S.-S. Guo, X.-B. Chen, and Y.-Z. Guo, "MicroRNA- 96-5p represses breast cancer proliferation and invasion through Wnt/β -catenin signaling via targeting CTNND1," Sci. Rep., vol. 10, no. 1, p. 44, Jan. 2020.

[35] I. Garrido-Cano, B. Pattanayak, A. Adam-Artigues, A. Lameirinhas, S. Torres-Ruiz, E. Tormo, R. Cervera, and P. Eroles, "MicroRNAs as a clue to overcome breast cancer treatment resistance," Cancer Metastasis Rev., vol. 41, no. 1, pp. 77–105, Mar. 2022.

[36] J. Hu, P. Su, M. Jiao, X. Bai, M. Qi, H. Liu, Z. Wu, J. Sun, G. Zhou, and B. Han, "TRPS1 suppresses breast cancer epithelial-mesenchymal transition program as a negative regulator of SUZ12," Transl. Oncol., vol. 11, no. 2, pp. 416–425, Apr. 2018.

[37] D. Lee, K. Apelt, S.-O. Lee, H.-R. Chan, M. S. Luijsterburg, J. W. C. Leung, and K. M. Miller, "ZMYM2 restricts 53BP1 at DNA double-strand breaks to favor BRCA1 loading and homologous recombination," Nucleic Acids Res., vol. 50, no. 7, pp. 3922–3943, Apr. 2022.

[38] C. Herrera-Pariente, L. Bonjoch, J. Muñoz, G. Fernàndez, Y. Soares de Lima, R. Mahmood, M. Cuatrecasas, T. Ocaña, S. Lopez-Prades, G. Llargués-Sistac, X. Domínguez-Rovira,J. Llach, I. Luzko, M. Díaz-Gay, C. Lazaro, J. Brunet, C. Castillo-Manzano, M. A. García-González, A. Lanas, M. Carrillo, R. Hernández San Gil, E. Quintero, N. Sala, G. Llort, L. Aguilera, L. Carot, P. Diez-Redondo, R. Jover, T. Ramon Y Cajal, J. Cubiella, A. Castells, F. Balaguer, L. Bujanda, S. Castellví-Bel, and L. Moreira, "CTNND1 is involved in germline predisposition to early-onset gastric cancer by affecting cell-to-cell interactions," Gastric Cancer, vol. 27, no. 4, pp. 747–759, Jul. 2024.

[39] Y. Ji, Z. Han, L. Shao, and Y. Zhao, "Evaluation of in vivo antitumor effects of low-frequency ultrasound-mediated miRNA-133a microbubble delivery in breast cancer," Cancer Med., vol. 5, no. 9, pp. 2534–2543, Sep. 2016.

[40] Z. Tian, H. Jiang, Y. Liu, Y. Huang, X. Xiong, H. Wu, and X. Dai, "MicroRNA-133b inhibits hepatocellular carcinoma cell progression by targeting sirt1," Exp. Cell Res., vol. 343, no. 2, pp. 135–147, May 2016.

[41] X. Liu and G. Li, "MicroRNA-133b inhibits proliferation and invasion of ovarian cancer cells through akt and erk1/2 inactivation by targeting epidermal growth factor receptor," International journal of clinical and experimental pathology, vol. 8, no. 9, pp. 10 605–10 614, 2015.

[42] S. Liu, S. Li, X. Yu, Q. Wang, and H. Sun, "microRNA-133b represses the progression of lung cancer through inhibiting SOX9/β -catenin signaling pathway," Int. J. Clin. Exp. Pathol., vol. 13, no. 9, pp. 2270–2279, Sep. 2020.

[43] T.-C. Huang, S. Renuse, S. Pinto, P. Kumar, Y. Yang, R. Chaerkady, B. Godsey, J. T. Mendell, M. K. Halushka, C. I. Civin, L. Marchionni, and A. Pandey, "Identification of mir-145 targets through an integrated omics analysis," Mol. Biosyst., vol. 11, no. 1, pp. 197–207, Jan. 2015.

[44] K.-M. Xiang and X.-R. Li, "MiR-133b acts as a tumor suppressor and negatively regulates TBPL1 in colorectal cancer cells," Asian Pac. J. Cancer Prev., vol. 15, no. 8, pp. 3767–3772, 2014.

[45] S. Huang, Q. Wa, J. Pan, X. Peng, D. Ren, Q. Li, Y. Dai, Q. Yang, Y. Huang, X. Zhang, W. Zhou, D. Yuan, J. Cao, Y. Li, P. He, and Y. Tang, "Transcriptional downregulation of mir-133b by REST promotes prostate cancer metastasis to bone via activating TGF-β signaling," Cell Death Dis., vol. 9, no. 7, Jul. 2018.

[46] X.-N. Chen, K.-F. Wang, Z.-Q. Xu, S.-J. Li, Q. Liu, D.-H. Fu, X. Wang, and B. Wu,"MiR-133b regulates bladder cancer cell proliferation and apoptosis by targeting bcl-w and akt1," Cancer Cell Int., vol. 14, no. 1, p. 70, Jul. 2014.

[47] Y.-T. Hua, W.-X. Xu, H. Li, and M. Xia, "Emerging roles of MiR-133a in human cancers," J. Cancer, vol. 12, no. 1, pp. 198–206, Jan. 2021.